First-principles investigation of the magnetic anisotropy and magnetic properties of Co/Ni(111) superlattices

F. Gimbert and L. Calmels*

CEMES, CNRS UPR 8011 and Université de Toulouse, 29 rue Jeanne Marvig, 31055 Toulouse, France

(Received 27 July 2012; published 7 November 2012)

We used first-principles methods to calculate the electronic and magnetic structure of Co/Ni(111) superlattices with a thickness of the Co and Ni layers ranging from one to four monolayers. We give a detailed database on the magnetocrystalline anisotropy energy induced by interfaces and on the total magnetic anisotropy energy including the shape anisotropy of the superlattices. The magnetic anisotropy is analyzed in terms of the anisotropy of the Co and Ni orbital magnetic moments and in terms of the electron states of the superlattices. Most of our results apply to superlattices with an fcc stacking of the atomic layers, but we also study the influence of stacking faults on the anisotropy. We describe the magnetization, and the density of states and spin polarization at the Fermi level of all these superlattices. The database which we provide should help researchers who aim to design Co/Ni–based magnetic or spintronic devices with suitable physical properties.

DOI: 10.1103/PhysRevB.86.184407 PACS number(s): 71.20.Be, 73.21.Cd, 75.30.Gw, 75.50.Cc

I. INTRODUCTION

Magnetic multilayers with perpendicular magnetic anisotropy (PMA) have been the subject of numerous studies because of their interesting potential applications in high-density magnetic recording and spintronic devices. They allow going beyond the superparamagnetic effect, which is a limit for longitudinal recording, giving access to magnetic media with smaller magnetic domains and a higher density.[1] Multilayers with PMA can also be used as magnetic electrodes in spin valves, the magnetic configuration of which can be changed by the spin-torque effect, using a spin-polarized electric current.[2–7] Taking advantage of this phenomenon should enable the design of spintronic devices in which the magnetic information would be written with local electric currents instead of magnetic fields. The spin transfer torque effect was first studied in spin valves based on magnetic layers with in-plane magnetization.[8–10] Recent research has shown that the critical current needed for switching a spin valve is lower for electrodes with out-of-plane than those with in-plane magnetic anisotropy.[11–15] This is due to the different roles played by the shape anisotropy and demagnetizing field in these two kinds of systems, for which the energy barriers between parallel and antiparallel states have different heights. The materials which have been the most intensively studied for their PMA properties are Co/Pd[16–21] and Co/Pt[20,22,23] multilayers.

Co/Ni multilayers have recently attracted attention as good candidates for PMA applications. Interest in these systems started with first-principles calculations which predicted that Co/Ni(111) superlattices may possess PMA.[24,25] These theoretical studies have also emphasized the importance of d_{xy} and $d_{x^2-y^2}$ electron states for the magnetic anisotropy of the superlattices. Experimental investigations have confirmed that Co/Ni sandwiches and superlattices with PMA can exist, and the maximum anisotropy has been found when the Co layers contain only one or two monolayers (MLs); the critical Co thickness above which the magnetic anisotropy is in-plane takes typical values near three or four MLs, depending on the sample quality and on the thickness of the Ni layers.[26–31]

Nanopillars containing spin valves with Co/Ni multilayers as magnetic electrodes have been used to study the spin transfer torque effect. The magnetization switching induced by an electric current has been demonstrated using Co/Ni electrodes with perpendicular anisotropy. It has, in particular, been shown that the critical current density is three or four times lower for Co/Ni electrodes terminated by Pt cap layers than for Co/Pt electrodes. The critical current is even lower when the Pt cap layers are not inserted during the growth process.[13,32] The efficiency of spin transfer torque in Co/Ni multilayers could be optimized by changing both the relative Co and Ni contents and the Co/Ni interface density. This would allow the control of the different parameters governing the torque.[13] The most important of these parameters are the magnetic anisotropy, which can be chosen either in-plane or out-of-plane, depending on the stacking; the Gilbert damping parameter α, which is relatively small in these materials[29,33,34] and does not depend strongly on the magnetic anisotropy, but on the relative concentration of Co and Ni atoms;[35] the density of states (DOS) and spin polarization at the Fermi level, which can be high in these materials[36] and should depend on the average composition and on the modification of the electronic structure induced by interfaces; and the magnetization of the superlattices, which can be chosen between that of bulk Ni and that of bulk Co. Recent studies have shown that the giant magnetoresistance of spin valves with Co/Ni electrodes is relatively high.[37] Co/Ni multilayers are also interesting because they can be used to reach PMA with only 3*d* transition metals, avoiding the use of heavy elements like Pt and Pd, which are responsible for high spin-orbit coupling.

Assessment of recent studies on Co/Ni multilayers clearly shows that these systems have mostly been studied experimentally.[26–31,38] Theoretical investigations which could help the interpretation of experimental data and of measured properties in terms of the electronic structure are rather rare. They mainly consist in a recent paper which compares the spin and orbital magnetic moments calculated *ab initio* and measured experimentally[39] and in two articles which describe the magnetic anisotropy energy (MAE) of only three different Co/Ni superlattices,[24,25] which is far from exhaustive. Systematic information on the most important parameters which must be known to understand the physical behavior of Co(n MLs)/Ni(p MLs) superlattices must be provided for the most

simple of these systems, for instance for $n = 1$–4 and $p = 1$–4. In this article we supply a detailed database on the MAE, magnetization, DOS and spin polarization at the Fermi level for a wide range of cobalt and nickel layer thicknesses in Co/Ni(111) superlattices. We also provide an interpretation of the magnetic anisotropy of these superlattices in terms of electron states and orbital magnetic moments. This database could further be used by researchers to interpret experimental data and to design devices with the required behavior.

II. COMPUTATIONAL DETAILS

We have calculated the electronic structure of Co(n MLs)/Ni(p MLs) superlattices with a (111) stacking axis using the first-principles code WIEN2K.[40] This code, which is based on the density functional theory (DFT), allows us to solve the Kohn-Sham equation with a linearized augmented plane-wave basis for expanding the one-particle wave functions. We used the parametrized equation proposed by Perdew and Wang[41] to express the exchange and correlation potential within the local spin density approximation. This approximation can indeed be considered as more efficient than the generalized gradient approximation for calculation of the MAE.[42] The maximum wave vector $K_{\max}$, which has been used for the plane-wave expansion of the Kohn-Sham wave functions in the interstitial area between atomic spheres, is given by the dimensionless parameter $RK_{\max} = 10$, where $R = 0.124$ nm is the radius which has been chosen for all the atoms of all the superlattices. The first Brillouin zone has been sampled with a typical number of 10 000 wave vectors. Previous studies have shown that such a dense mesh must be used to calculate the magnetocrystalline anisotropy energy (MCAE; which we define as the difference in the superlattice energies calculated with the magnetization parallel versus perpendicular to the interfaces) with a reasonable accuracy,[24] and we checked that this accuracy is, in our case, about 0.05 meV/unit cell. The same k-mesh fineness has been used when the magnetization is parallel or perpendicular to interfaces, even if the superlattice space group and explicit list of wave vectors depend on the direction of the magnetization. The electronic structure is first calculated without including spin-orbit coupling effects. The result of this initial calculation is further used to compute the energy correction induced by the spin-orbit interaction within the scalar relativistic approximation [we chose to include unoccupied states up to a maximum energy of 7 Rydbergs (Ryd) above the Fermi level in this calculation based on the second-order perturbation theory].

For most of the Co(n MLs)/Ni(p MLs) superlattices, we considered a face-centered cubic (fcc) stacking of atomic layers,[43] with the same distance between all the successive atomic layers and a lattice parameter $a = (n\sqrt{2}a_{\mathrm{Co}} + pa_{\mathrm{Ni}})/(n + p)$ given by the Vegard law, using the lattice constants $a_{\mathrm{Ni}} = 0.352$ nm and $a_{\mathrm{Co}} = 0.251$ nm of bulk fcc Ni and bulk hcp Co. We performed atomic layer relaxation on some of these superlattices: the calculated relaxation is so small (the distance between atomic layers being nearly the same in bulk Ni and bulk Co) that it does not significantly change the values of the spin magnetic moments or of the MAE. In the following we consider the Ox, Oy, and Oz axes as, respectively, parallel to the $[\bar{1}10]$, $[\bar{1}\bar{1}2]$, and [111] directions of the fcc stacking.

III. MAGNETIC ANISOTROPY ENERGY OF THE Co/Ni(111) SUPERLATTICES

Two phenomena contribute to the MAE of magnetic multilayers. The first contribution is the magnetocrystalline anisotropy (MCA), which expresses the fact that the matrix elements of the spin-orbit coupling Hamiltonian and the ground-state energy of the crystal depend on the direction of the magnetization with respect to the crystal axes. The MCA exists in bulk magnetic crystals and can be strongly enhanced by interfaces. The second contribution to the magnetic anisotropy is due to interaction between magnetic dipoles located at different atomic sites. This contribution, also called shape anisotropy since it depends on the shape of the sample, must be calculated by summing all the dipole-dipole interaction energies. It gives a negative contribution to the MAE and favors in-plane magnetization in the case of thin magnetic layers and multilayers. The shape anisotropy energy can be calculated considering explicitly discrete dipoles, as shown by Daalderop, who obtained a contribution of -0.08 meV per Co atom and -0.01 meV per Ni atom of the Co/Ni superlattices.[24] It can also be calculated considering that the magnetic layers are made of uniform materials; in this case, the shape anisotropy energy is given by

$$\mathrm{E_{Shape}} = -t_{\mathrm{Co}}\left(\frac{1}{2}\mu_0\mathcal{M}_{\mathrm{Co}}^2\right) - t_{\mathrm{Ni}}\left(\frac{1}{2}\mu_0\mathcal{M}_{\mathrm{Ni}}^2\right), \qquad (1)$$

where t_{Co}, t_{Ni}, $\mathcal{M}_{\mathrm{Co}}$, and $\mathcal{M}_{\mathrm{Ni}}$ are, respectively, the Co and the Ni total thicknesses and magnetizations in the superlattices. For compact stackings like Co/Ni(111) superlattices with an fcc structure, Eq. (1) gives numerical values in very good agreement with those calculated by Daalderop for discrete dipoles. In the following, the shape anisotropy is always calculated using the numerical results of Daalderop.

Before describing in detail our results on the MAE of Co(n MLs)/Ni(p MLs) superlattices, we compare in Table I some of these energies with the few theoretical and some of the experimental data available in the literature. The MCAE which we calculated for Co(1 ML)/Ni(2 MLs), Co(1 ML)/Ni(5 MLs), and Co(2 MLs)/Ni(1 ML) is of the same order of magnitude as those calculated by Daalderop[24] and Kyuno:[25] the MCAE is stronger and positive for Co(1 ML)/Ni(2 MLs), smaller for Co(1 ML)/Ni(5 MLs), and slightly negative for Co(2 MLs)/Ni(1 ML). The differences which appear between our results and those from the literature are mainly due to the fact that we used a code based on the linearized augmented plane-wave method, while Daalderop and Kyuno used codes based on the linearized muffin-tin orbital method. The MCAE that we calculated for Co(1 ML)/Ni(3 MLs), Co(2 MLs)/Ni(3 MLs), Co(3 MLs)/Ni(3 MLs), and Co(4 MLs)/Ni(3 MLs) is positive and of the same order of magnitude as the MCAE deduced from experimental measurements,[31] except maybe for the superlattice Co(2 MLs)/Ni(3 MLs), for which the calculated MCAE is smaller than the experimental result (a possible explanation for this small discrepancy is given in Sec. VI).

Figure 1(a) shows the MCAE per Co(n MLs)/Ni(p MLs) superlattice unit cell, calculated as a function of the Co layer

TABLE I. Magnetocrystalline anisotropy energy (MCAE; in meV/unit cell) for the superlattices Co(1 ML)/Ni(2 MLs), Co(1 ML)/Ni(5 MLs), and Co(2 MLs)/Ni(1 ML), for which our results are compared to those calculated by Daalderop[24] and Kyuno,[25] and for the superlattices Co(1 ML)/Ni(3 MLs), Co(2 MLs)/Ni(3 MLs), Co(3 MLs)/Ni(3 MLs), and Co(4 MLs)/Ni(3 MLs), for which our results are compared to those deduced from magnetometry experiments.[31]

	Calculated MCAE			
Superlattice	Daalderop[24]	Kyuno[25]	Measured MCAE: Gottwald[31]	Our results
Co(1 ML)/Ni(2 MLs)	0.31	0.35	–	0.45
Co(1 ML)/Ni(5 MLs)	0.14	–	–	0.25
Co(2 MLs)/Ni(1 ML)	− 0.04	–	–	− 0.12
Co(1 ML)/Ni(3 MLs)	–	–	0.32	0.4
Co(2 MLs)/Ni(3 MLs)	–	–	0.34	0.11
Co(3 MLs)/Ni(3 MLs)	–	–	0.35	0.29
Co(4 MLs)/Ni(3 MLs)	–	–	0.34	0.29

thickness and for several Ni layer thicknesses. The MCAE is positive and does not depend strongly on the Ni layer thickness when $t_{Ni} \geqslant 2$ MLs. The situation is different for Co(n MLs)/Ni(1 ML) superlattices, which show lower MCAE values and a strong tendency towards in-plane magnetic anisotropy. In any cases, the MCAE is maximum when the Co layers only contain one atomic plane, and the maximum is obtained for Co(1 ML)/Ni(2 MLs) and Co(1 ML)/Ni(3 MLs). The MCAE shows slight oscillations as a function of the Co layer thickness, with a minimum value when $t_{Co} = 2$ MLs.

The total MAE per unit cell of the same superlattices is described in Fig. 1(b). The MAE decreases rapidly with the Co thickness, the negative contribution of the shape anisotropy becoming more and more important. All the superlattices show in-plane anisotropy when $t_{Co} \geqslant 4$ MLs.

The results presented in Fig. 1 describe the MAE per unit cell of different Co/Ni(111) superlattices. The energies reported in that figure describe superlattices with different periods; it also seems pertinent to compare the K_{eff} values calculated for the different multilayers and shown in Fig. 2. K_{eff} is the MAE per surface unit and per thickness unit of the superlattices. In real Co/Ni superlattices, an additional magnetocrystalline contribution would appear because of the interfaces between the superlattices and the substrate and cap layers. Figure 2 shows that positive values of K_{eff} are mostly obtained for Co(1 ML)/Ni(p MLs) superlattices, for which the MCA contribution to K_{eff} is the highest. The shape anisotropy contribution to K_{eff} is of course always negative and suppresses the perpendicular anisotropy when the relative content of Co atoms is high enough. K_{eff} is slightly negative for most of the superlattices, except for Co(2 MLs)/Ni(1 ML), Co(4 MLs)/Ni(1 ML), and Co(3 MLs)/Ni(1 ML), which possess a strong in-plane anisotropy, and for Co(1 ML)/Ni(2 MLs), Co(1 ML)/Ni(3 MLs), Co(1 ML)/Ni(4 MLs), and Co(1 ML)/Ni(1 ML), which show strong perpendicular anisotropy. The latter superlattices have, at the same time, a high interface density and a high Ni content.

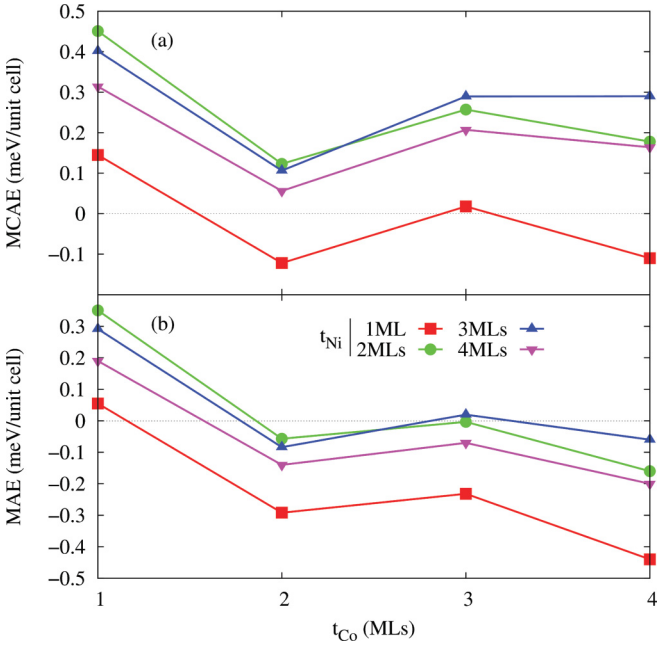

FIG. 1. (Color online) (a) Magnetocrystalline anisotropy energy per unit cell and (b) magnetic anisotropy energy per unit cell for Co(n MLs)/Ni(p MLs) superlattices as a function of the Co layer thickness t_{Co} and for several Ni layer thicknesses t_{Ni}.

IV. INTERPRETATION OF THE MCAE IN TERMS OF ORBITAL MOMENTS

The physical origin of the MCAE of Co/Ni(111) superlattices is not obvious and must be studied in detail. The

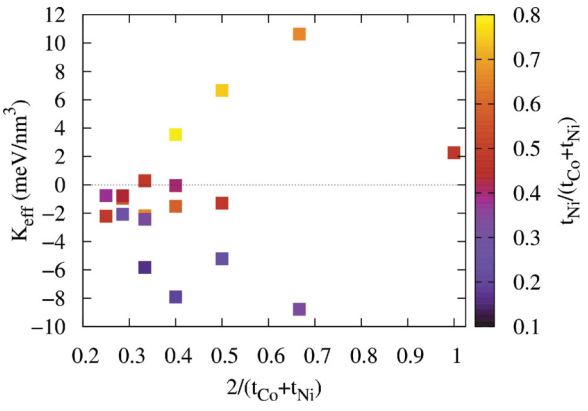

FIG. 2. (Color online) Magnetic anisotropy energy K_{eff} per surface unit and per thickness unit of Co(n MLs)/Ni(p MLs) superlattices, as a function of the interface density $\frac{2}{t_{Co}+t_{Ni}}$ and relative Ni content $\frac{t_{Ni}}{t_{Co}+t_{Ni}}$.

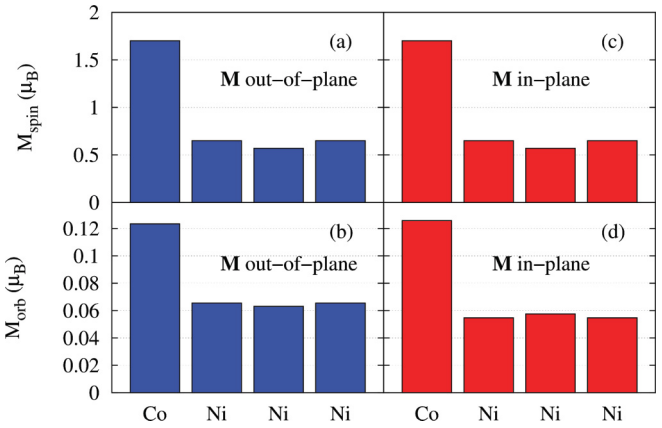

FIG. 3. (Color online) Spin and orbital magnetic moments of the Co and Ni atoms in a period of the Co(1 ML)/Ni(3 MLs) superlattice: (a), (b) when the magnetization is perpendicular to interfaces and (c), (d) when the magnetization is parallel to interfaces.

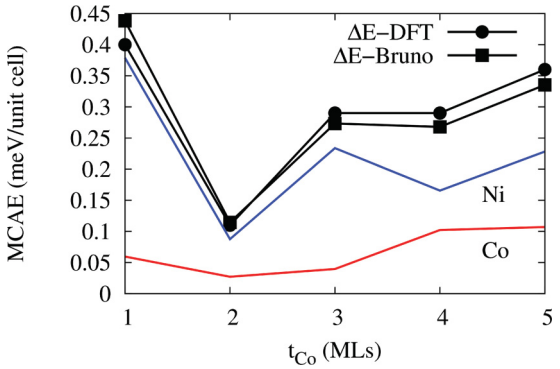

FIG. 4. (Color online) Magnetocrystalline anisotropy energy of Co(n MLs)/Ni(3 MLs) superlattices, obtained from the difference between the ground-state energies calculated for magnetization perpendicular and parallel to interfaces (ΔE–DFT) and those calculated from the Bruno model (ΔE–Bruno). The contributions of Ni and Co atoms are also shown.

values presented in the previous section show that the MCAE is considerably higher for Co/Ni superlattices than for bulk fcc Ni and hcp Co.[44] This enhancement of the MCAE is due to the Co/Ni interfaces which modify the interaction between the electron angular momentum and the crystal.[45]

Figure 3 shows the values of the spin and orbital magnetic moments of the different atoms in the period of the Co(1 ML)/Ni(3 MLs) superlattice, for different directions of the magnetization and as a function of the atomic layer index. These spin magnetic moments have been calculated from the difference between the number of majority- and the number of minority-spin electrons inside muffin-tin spheres. The spin magnetic moments show negligible anisotropy, while the orbital magnetic moments are clearly higher where the magnetization is perpendicular to the interfaces. This is in agreement with the theoretical model developed by Bruno[46] for magnetic metals with the majority-spin d bands below the Fermi level. This model expresses the MCAE of Co(n MLs)/Ni(p MLs) superlattices in terms of the anisotropy of the Ni and Co orbital magnetic moments. It can be described by the following equation:

$$\mathrm{MCAE} = \frac{p}{4\mu_B}\xi_{\mathrm{Ni}}[\mathrm{M}^{\downarrow}_{\mathrm{orb}}(\mathrm{Ni})(\perp) - \mathrm{M}^{\downarrow}_{\mathrm{orb}}(\mathrm{Ni})(\parallel)] + \frac{n}{4\mu_B}\xi_{\mathrm{Co}}[\mathrm{M}^{\downarrow}_{\mathrm{orb}}(\mathrm{Co})(\perp) - \mathrm{M}^{\downarrow}_{\mathrm{orb}}(\mathrm{Co})(\parallel)], \quad (2)$$

where $\xi_{\mathrm{Ni}} = 100$ meV, $\xi_{\mathrm{Co}} = 86$ meV,[47,48] and μ_B is the Bohr magneton. $\mathrm{M}^{\downarrow}_{\mathrm{orb}}(\mathrm{Ni})(\perp)$, $\mathrm{M}^{\downarrow}_{\mathrm{orb}}(\mathrm{Ni})(\parallel)$, $\mathrm{M}^{\downarrow}_{\mathrm{orb}}(\mathrm{Co})(\perp)$, and $\mathrm{M}^{\downarrow}_{\mathrm{orb}}(\mathrm{Co})(\parallel)$ give the contribution of minority-spin electrons to the averaged orbital magnetic moment of Ni and Co atoms in the superlattices, for magnetization perpendicular and parallel to interfaces, respectively. Details on the calculation of the orbital magnetic moments have been published recently.[39]

Figure 4 compares the values of the MCAE of Co(n MLs)/Ni(3 MLs) superlattices, calculated from the difference between the ground-state energies when magnetization is perpendicular and parallel to interfaces and the ground-state energies calculated with the Bruno model. The agreement between the MCAEs calculated by these two methods is surprisingly good. Moreover, the Bruno model shows that the contribution of Ni atoms to the MCAE is higher than that of Co atoms, even when the number of Co atomic layers becomes high.

V. INTERPRETATION OF THE MCAE IN TERMS OF ELECTRON STATES

We have analyzed the modification of the electronic structure induced by spin-orbit coupling as a function of the direction of the magnetization, in order to establish a correlation between the MCA and the electron states of the Co/Ni(111) superlattices. First, we have inspected the magnetization dependence of the superlattice band structure, to search for the most important degeneracy lifting which may lower the ground-state energy for a given orientation of the magnetization. Degeneracy lifting between d bands can contribute to the magnetic anisotropy if several conditions are fulfilled: the degenerated d bands must have an energy very close to the Fermi level (this condition ensures that their occupation changes after degeneracy lifting), if possible with a weak dispersion along one of the high-symmetry directions of the first Brillouin zone.[49] We have calculated the band structure of several Co(n MLs)/Ni(p MLs) superlattices and searched for possible degeneracy lifting at E_F. For most of the superlattices, the lifting occurs either above or below E_F, which does not strongly affect the ground-state energy, and degeneracy lifting at the Fermi level is very rare.

Figure 5 shows the band structure of the superlattice Co(2 MLs)/Ni(4 MLs) when the magnetization is in-plane [Fig. 5(a)] and out of plane [Fig. 5(b)]. The energy and wave vectors at which degeneracy lifting can be observed depend on the magnetization direction. The degeneracy lifting mostly happens between bands which would simply cross each other if spin-orbit coupling were ignored. The most important lifting can be observed for magnetization perpendicular to the interfaces. In this case, the degeneracy between flat d bands is lifted along the whole Γ-A direction. One of these lifting occurs exactly at E_F when the magnetization is out of plane, lowering the energy of one band while the other band becomes unoccupied. The corresponding two bands (which are linear combinations of Ni d_{xz} and d_{yz} atomic orbitals)

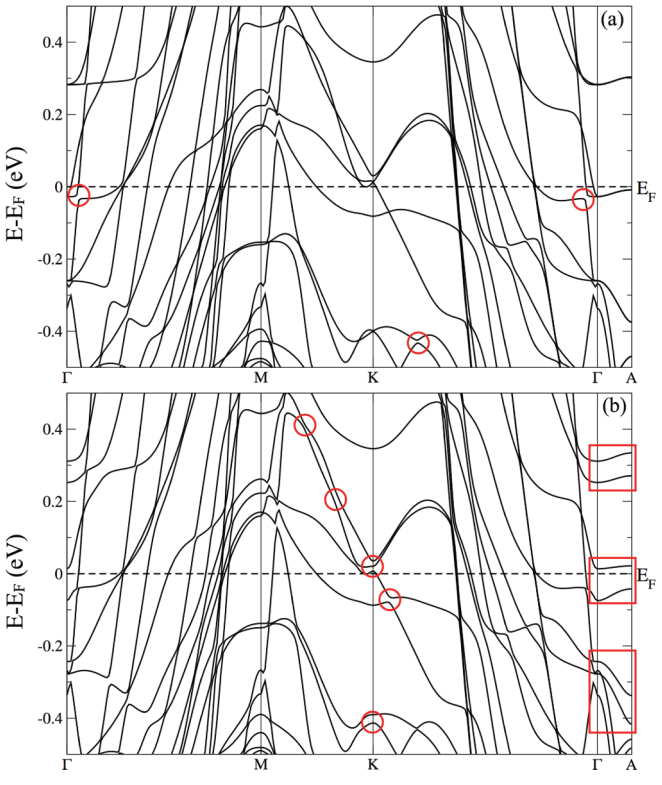

FIG. 5. (Color online) Band structure of the Co(2 MLs)/Ni (4 MLs) superlattice for magnetization (a) parallel and (b) perpendicular to the interfaces. The (red) circles and squares show the most important degeneracy lifting induced by spin-orbit coupling.

are degenerated with a very low negative energy for in-plane magnetization. Even for this superlattice, which shows a clear band lifting at E_F, the sign of the MCAE cannot, however, be predicted only from the analysis of the band degeneracy lifting induced by spin-orbit coupling.

To better understand the sign of the MCAE, we must calculate the ground-state energy correction induced by spin-orbit coupling in the second-order perturbation theory and identify the electron states which make the most important contribution to this correction. The ground-state energy correction is given by

$$\Delta E = \sum_{E_{n\mathbf{k}}<E_F} \sum_{E_{n'\mathbf{k}}>E_F} \frac{|\langle\psi_{n\mathbf{k}}|\hat{H}_{\mathrm{SO}}|\psi_{n'\mathbf{k}}\rangle|^2}{E_{n\mathbf{k}} - E_{n'\mathbf{k}}}. \quad (3)$$

The matrix elements of the spin-orbit-coupling Hamiltonian which appear in Eq. (3) couple occupied and unoccupied Bloch states with the same Bloch vector $\mathbf{k}$. The value of ΔE depends on the magnetization direction, and the virtual transitions which appear in this equation strongly contribute when they couple occupied and unoccupied states close to the Fermi level. The Bloch states coupled by these virtual transitions can be linear combinations of the same or of different d atomic orbitals. They can have the same (majority or minority) or different spin states. Each of these Bloch states can be characterized by the value of its magnetic quantum number m_l ($|m_l|$ being equal to 0 for d_{z^2}, 1 for d_{xz} and d_{yz}, and 2 for d_{xy} and $d_{x^2-y^2}$ orbitals) and spin quantum number $m_s = \pm 1/2$; a virtual transition can be described by the variations Δm_l and Δm_s of these quantum numbers. The virtual transitions which actually contribute to ΔE are those with nonvanishing $\langle\psi_{n\mathbf{k}}|\hat{H}_{\mathrm{SO}}|\psi_{n'\mathbf{k}}\rangle$ and with particular values of Δm_s and Δm_l. The sign and the amplitude of the contribution of a virtual transition depend on the magnetization direction, parallel or perpendicular to the atomic layers. Daalderop[50] proposed simple rules which can be used to understand which virtual transitions favor in-plane or out-of-plane magnetization (see also the Appendix). The virtual transitions which favor in-plane anisotropy are those between states with $\Delta|m_l| = 0$ and different spin or between states with $\Delta|m_l| = \pm 1$ and the same spin. The virtual transitions which favor perpendicular anisotropy are those between states with $\Delta|m_l| = 0$ and same spin or between states with $\Delta|m_l| = \pm 1$ and opposite spin.

Previous studies used these simple rules to identify the electron states responsible for the magnetic anisotropy of thin Co layers from the peaks in the m_l-resolved majority- and minority-spin DOS curves.[50,51] Such an analysis turns out to be difficult in our case because we can, at the same time, identify DOS peaks involved in virtual transitions favoring in-plane anisotropy, and DOS peaks favoring out-of-plane anisotropy. To obtain unambiguous information on the most important electron states which are responsible for the actual anisotropy, we must focus on the most important of the virtual transitions mentioned above. The transitions which give the highest contribution have been identified in the article by Kyuno *et al.*[25] (see also the Appendix). Among all the virtual transitions favoring in-plane anisotropy, the most important are those between states with $m_l = 0$ and $|m_l| = 1$ with the same spin and those between states with $|m_l| = 2$ and different spin. Conversely, the most important transitions favoring perpendicular anisotropy are those between states with $m_l = 0$ and states with $|m_l| = 1$ and different spin and those between states with $|m_l| = 2$ and the same spin. These restricted rules can, for instance, be used to understand, from partial DOS curves, why the magnetic anisotropy is perpendicular for Co(1 ML)/Ni(2 MLs) and in-plane for Co(2 MLs)/Ni(1 ML). The m_l-resolved DOS curves for a Co atom of these two superlattices are shown in Figs. 6 and 7, respectively. For Co(1 ML)/Ni(2 MLs), we can identify important $\{m_l = 0 \rightarrow |m_l| = 1\}$ and $\{|m_l| = 1 \rightarrow m_l = 0\}$ virtual transitions from majority-spin states at -0.7 eV to minority-spin states near 0.55 eV; these transitions promote perpendicular anisotropy. Similar virtual transitions can also be observed for Co(2 MLs)/Ni(1 ML), but they will give a lower contribution since the density of unoccupied minority-spin states is lower and at a slightly higher energy (near 0.9 eV). Similarly, we can identify important virtual transitions between occupied majority-spin (near -0.7 eV) and unoccupied minority-spin (near 1.0 eV) states with $|m_l| = 2$. These virtual transitions promote in-plane anisotropy for the superlattice Co(2 MLs)/Ni(1 ML). Figure 6 shows that similar virtual transitions would have a lower contribution in Co(1 ML)/Ni(2 MLs) because the unoccupied minority-spin DOS peak is lower for this superlattice. Similar conclusions could be drawn from the partial DOS curves calculated for Ni atoms, which emphasize the importance of atomic orbitals with quantum numbers $|m_l| = 1$ and $|m_l| = 2$ for explaining the magnetic anisotropy of the Co/Ni(111) superlattices. We have checked, in the band structure of these two superlattices, shown in Figs. 8 and 9, respectively, that

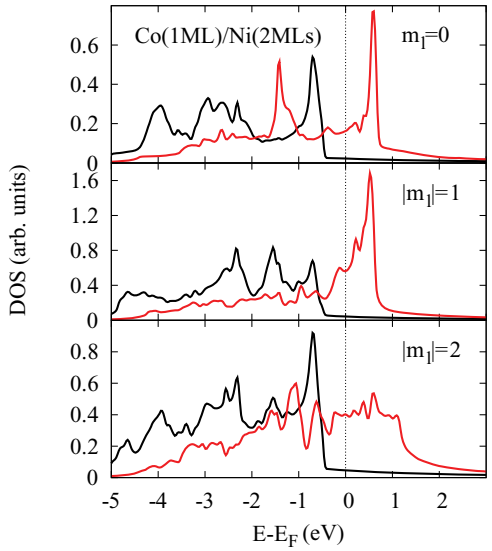

FIG. 6. (Color online) m_l-resolved density of states (DOS) for a Co atom of the superlattice Co(1 ML)/Ni(2 MLs), for majority spin (black curves) and minority spin [light (red) curves].

all the DOS peaks mentioned above correspond to virtual transitions with the same Bloch vector. The most important Bloch vectors contributing to the virtual transitions are near M and between K and Γ.

VI. INFLUENCE OF THE ATOMIC LAYER STACKING ON THE MCAE

In Sec. III, we mentioned that the MCAE calculated by first-principles methods is in rather good agreement with values deduced from experimental measurements,[31] except when the thickness of the Co layers is 2 MLs (the calculated MCAE is, in this case, smaller than the experimental value). We tried to understand if this small disagreement could be due to the atomic layer stacking, and we calculated the MCAE for

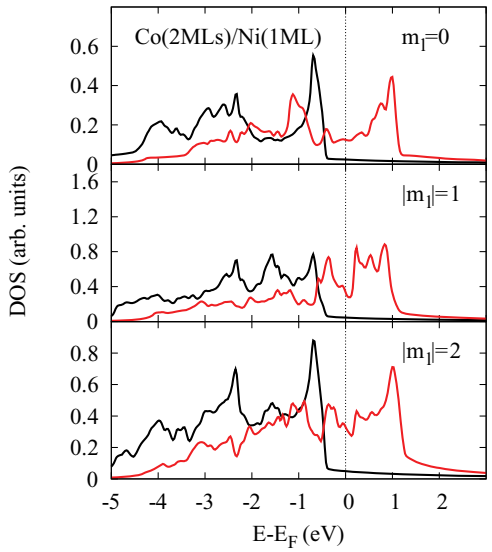

FIG. 7. (Color online) Same as Fig. 6, but for the superlattice Co(2 MLs)/Ni(1 ML).

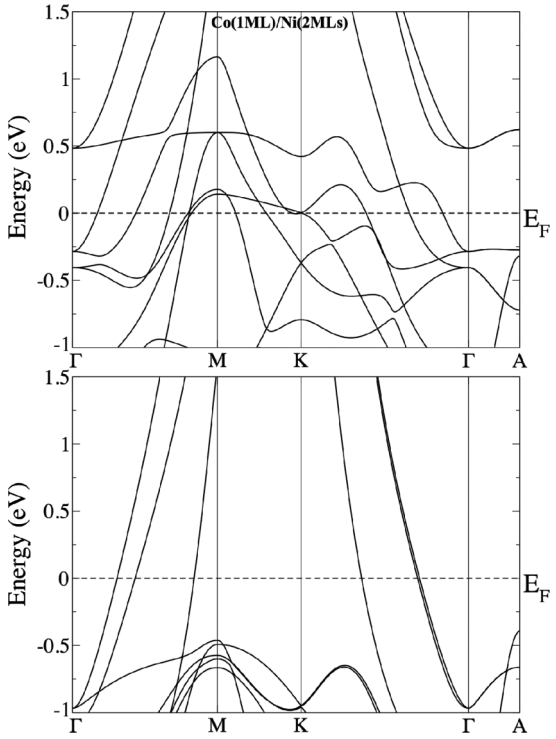

FIG. 8. Majority spin (lower panel) and minority spin (upper panel) band structure of the superlattice Co(1 ML)/Ni(2 MLs).

Co(n MLs)/Ni(3 MLs) superlattices with several possible atomic structures, ranging from pure fcc to pure hcp.

Figure 10 shows the value of the MCAE calculated for these superlattices, as a function of the thickness of the Co layers, for pure fcc superlattices (ABC stacking of the atomic layers), pure hcp superlattices (AB stacking), and intermediate stacking (labeled fcchcp), in which the crystal structure is fcc for all the Ni and hcp for all the Co atomic layers; this corresponds, for instance, to the stacking $Ni_ANi_BNi_CCo_ANi_CNi_BNi_ACo_C$ for Co(1 ML)/Ni(3 MLs), to the stacking $Ni_ANi_BNi_CCo_ACo_C$ for Co(2 MLs)/Ni(3 MLs), or to the stacking $Ni_ANi_BNi_CCo_ACo_CCo_ANi_CNi_BNi_ACo_CCo_ACo_C$ for Co(3 MLs)/Ni(3 MLs). The stackings with the lowest MCAE are those with the lowest ground-state energy [i.e., fcc stacking for Co(1 ML)/Ni(3 MLs), and fcchcp stacking for Co(2 MLs)/Ni(3 MLs), Co(3 MLs)/Ni(3 MLs), and Co(4 MLs)/Ni(3 MLs)]. Figure 10 shows that the variations in the MCAE as a function of the Co layer thickness are made smoother when we only consider the superlattice structure with the lowest ground-state energy: in the case of fcchcp stacking, the MCAE regularly decreases with Co thickness and does not show the oscillation which was observed for a Co thickness of 2 MLs for the pure fcc structure. Consequently, the small disagreement between calculated and measured values of the MCAE may be due to the fact that some of the samples used in experiments could possess stacking faults. We mention that the ground-state energy of the different superlattices has been represented in Fig. 10 after subtraction of the energy which would be that of the Co and Ni atoms in bulk fcc Ni and bulk hcp Co, in order to represent the ground-state energy of all the superlattices in the same figure.

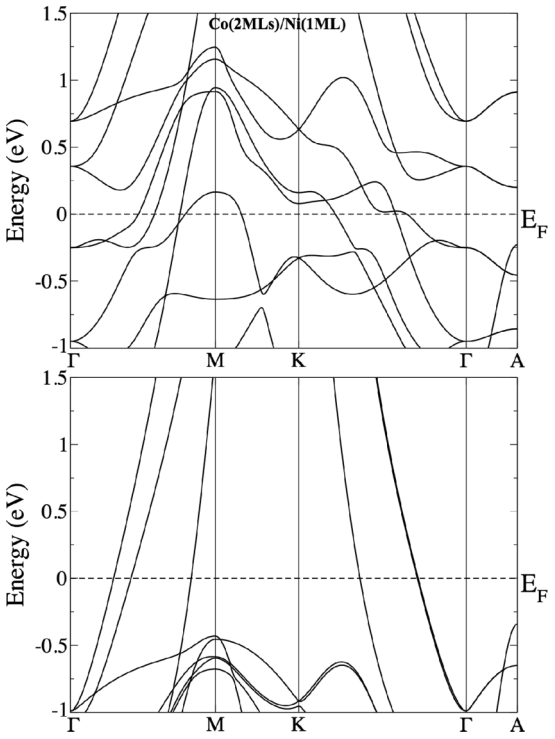

FIG. 9. Same as Fig. 8, but for the superlattice Co(2 MLs)/Ni (1 ML).

VII. MAGNETIZATION, DENSITY OF STATES AND SPIN POLARIZATION AT THE FERMI LEVEL

First-principles calculations and x-ray magnetic circular dichroism experiments have recently been used to get information on the values of the spin and orbital magnetic moments in Co/Ni(111) superlattices.[39] This study showed

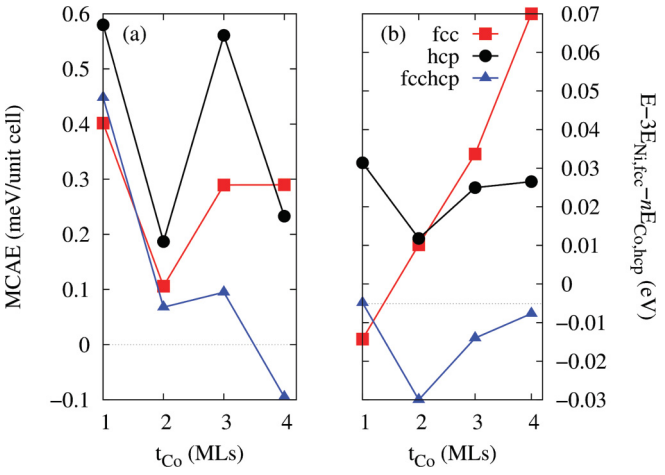

FIG. 10. (Color online) (a) Magnetocrystalline anisotropy energy for Co(n MLs)/Ni(3 MLs) superlattices, as a function of the Co layer thickness and for different stackings of the atomic layers (pure fcc, pure hcp, and an intermediate situation where the stacking is fcc for Ni and hcp for Co layers). (b) Ground-state energy per unit cell of the same superlattices; in order to represent all the results in the same graph, the energy of three Ni atoms in bulk fcc Ni and n Co atoms in bulk hcp Co has been subtracted from the ground-state energy of the Co(n MLs)/Ni(3 MLs) superlattices.

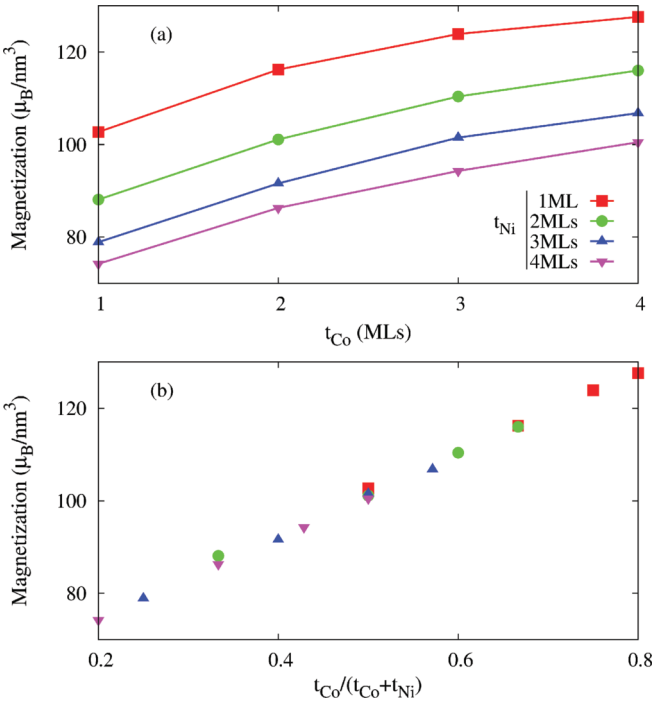

FIG. 11. (Color online) Magnetization of Co(n MLs)/Ni(p MLs) superlattices: (a) as a function of the Co layer thickness t_{Co} and for several Ni layer thicknesses t_{Ni} and (b) as a function of the Co content.

that the spin magnetic moment of the different Co and Ni atoms does not depend strongly on the location of these atoms (at the center of a layer or close to an interface) and that the spin magnetic moment is considerably higher than the orbital magnetic moment. We can further estimate the magnetization of the superlattices neglecting the contribution of the

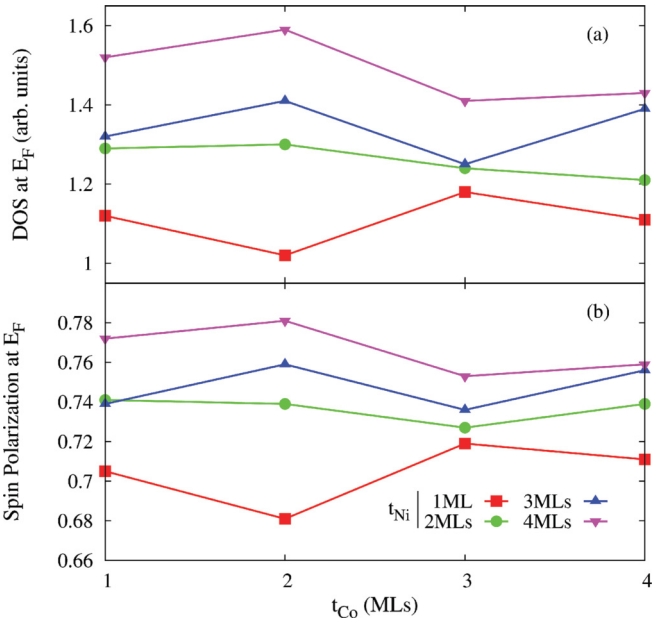

FIG. 12. (Color online) (a) Density of states (DOS) at the Fermi level and (b) spin polarization at the Fermi level for Co(n MLs)/Ni(p MLs) superlattices, as a function of the Co layer thickness and for several Ni layer thicknesses.

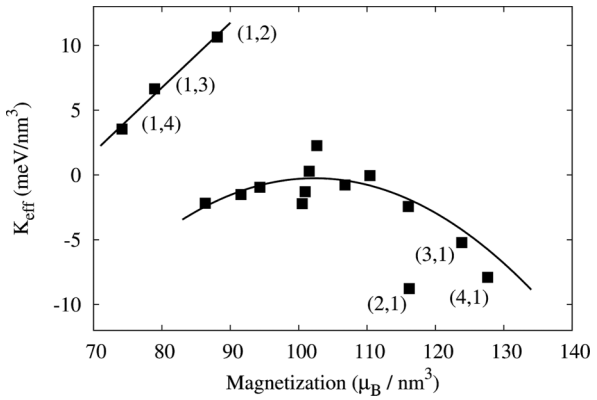

FIG. 13. Magnetic anisotropy energy per surface unit and per thickness unit as a function of the magnetization of Co(n MLs)/Ni(p MLs) superlattices. The values (n,p) are indicated for some of these superlattices.

orbital magnetic moments. Interface effects on the spin magnetic moments being small, the calculated magnetization varies more or less linearly as a function of the relative Co content, between the value calculated for bulk fcc Ni and that calculated for bulk fcc Co, as shown in Fig. 11.

These values of the magnetization have been calculated from the energy integration of the majority- and minority-spin total DOS, up to the Fermi level. Energy-resolved results are also interesting for the interpretation of experiments. In particular, the DOS and spin polarization at the Fermi level are important parameters which must be known for interpretation of the transport and magnetotransport experiments and for analysis of the spin-torque effect. Figure 12(a) shows the calculated DOS at the Fermi level, represented as a function of the Co layer thickness and for several Ni layer thicknesses. This DOS increases with the relative Ni content. For a given value of the relative Ni content, the DOS at the Fermi level also increases when the density of interfaces decreases: it is, for instance, higher for Co(4 MLs)/Ni(4 MLs) than for Co(1 ML)/Ni(1 ML). When the thickness of the Co layers becomes high, the DOS at E_F does not depend strongly on the thickness of the Ni layers. Figure 12(b) shows the spin polarization at the Fermi level versus the Co and Ni layer thicknesses. It shows the same kind of variations as the DOS curves described in Fig. 12(a).

VIII. DISCUSSION AND CONCLUSION

The results presented in the previous sections have shown that most of the Co(n MLs)/Ni(p MLs) superlattices possess a moderate or weak parallel anisotropy, except for the superlattices Co(2 MLs)/Ni(1 ML), Co(4 MLs)/Ni(1 ML), and Co(3 MLs)/Ni(1 ML), which show a strong parallel anisotropy. Only four superlattices possess a PMA which is strong for Co(1 ML)/Ni(2 MLs), intermediate for Co(1 ML)/Ni(3 MLs), and weaker for Co(1 ML)/Ni(4 MLs) and Co(1 ML)/Ni(1 ML). These superlattices present a wide range of magnetizations, DOS and spin polarizations at the Fermi level, which can all be adjusted by changing the relative Co and Ni content and by choosing the density of Co/Ni interfaces in the multilayers. All these parameters, and the strength and sign of the magnetic anisotropy, can be chosen independently in order to optimize the Co/Ni superlattices used for specific applications in devices. As an example, we can adjust the Ni content and interface density to choose, at the same time, the MAE and the magnetization. This is illustrated in Fig. 13, where $K_{\rm eff}$ is represented as a function of the magnetization $\mathcal{M}$, for all the superlattices described above. In this figure, most of the data $K_{\rm eff}(\mathcal{M})$ can be fitted by a curve with a parabolic shape, except for the three superlattices which present the strongest perpendicular anisotropy. Figure 13 shows that, in some cases, we have access to superlattices with the same magnetization but different magnetic anisotropies or to superlattices with the same magnetic anisotropy but different magnetizations.

To summarize, we have presented a wide database which describes the physical properties of Co(n MLs)/Ni(p MLs) superlattices with an fcc stacking of the (111) atomic layers. We have given details on the MCAE, the MAE, the magnetization, the DOS and spin polarization at the Fermi level. This database could be useful for researchers who want to design magnetic or spintronic devices containing Co/Ni superlattices for specific applications or in which the efficiency of the spin-torque effect could be adjusted.

ACKNOWLEDGMENT

The calculations presented in this article were performed at the CALMIP/UPS Toulouse parallel computer center.

TABLE II. Nonvanishing $\langle d_i,m_s|\hat{H}_{\rm SO}|d_{i'},m_{s'}\rangle$ matrix elements.

	$\lvert z^2,+\frac{1}{2}\rangle$	$\lvert z^2,-\frac{1}{2}\rangle$	$\lvert yz,+\frac{1}{2}\rangle$	$\lvert yz,-\frac{1}{2}\rangle$	$\lvert xz,+\frac{1}{2}\rangle$	$\lvert xz,-\frac{1}{2}\rangle$	$\lvert xy,+\frac{1}{2}\rangle$	$\lvert xy,-\frac{1}{2}\rangle$	$\lvert x^2-y^2,+\frac{1}{2}\rangle$	$\lvert x^2-y^2,-\frac{1}{2}\rangle$
$\langle z^2,+\frac{1}{2}\rvert$				$i\frac{\sqrt{3}}{2}\xi\hbar^2$		$-\frac{\sqrt{3}}{2}\xi\hbar^2$				
$\langle z^2,-\frac{1}{2}\rvert$			$i\frac{\sqrt{3}}{2}\xi\hbar^2$		$\frac{\sqrt{3}}{2}\xi\hbar^2$					
$\langle yz,+\frac{1}{2}\rvert$		$-i\frac{\sqrt{3}}{2}\xi\hbar^2$			$i\frac{1}{2}\xi\hbar^2$			$-\frac{1}{2}\xi\hbar^2$		$-i\frac{1}{2}\xi\hbar^2$
$\langle yz,-\frac{1}{2}\rvert$	$-i\frac{\sqrt{3}}{2}\xi\hbar^2$					$-i\frac{1}{2}\xi\hbar^2$	$\frac{1}{2}\xi\hbar^2$		$-i\frac{1}{2}\xi\hbar^2$	
$\langle xz,+\frac{1}{2}\rvert$		$\frac{\sqrt{3}}{2}\xi\hbar^2$	$-i\frac{1}{2}\xi\hbar^2$					$i\frac{1}{2}\xi\hbar^2$		$-\frac{1}{2}\xi\hbar^2$
$\langle xz,-\frac{1}{2}\rvert$	$-\frac{\sqrt{3}}{2}\xi\hbar^2$			$i\frac{1}{2}\xi\hbar^2$			$i\frac{1}{2}\xi\hbar^2$		$\frac{1}{2}\xi\hbar^2$	
$\langle xy,+\frac{1}{2}\rvert$				$\frac{1}{2}\xi\hbar^2$		$-i\frac{1}{2}\xi\hbar^2$			$i\xi\hbar^2$	
$\langle xy,-\frac{1}{2}\rvert$			$-\frac{1}{2}\xi\hbar^2$		$-i\frac{1}{2}\xi\hbar^2$					$-i\xi\hbar^2$
$\langle x^2-y^2,+\frac{1}{2}\rvert$				$i\frac{1}{2}\xi\hbar^2$		$\frac{1}{2}\xi\hbar^2$	$-i\xi\hbar^2$			
$\langle x^2-y^2,-\frac{1}{2}\rvert$			$i\frac{1}{2}\xi\hbar^2$		$-\frac{1}{2}\xi\hbar^2$			$i\xi\hbar^2$		

TABLE III. Nonvanishing values of $\{|\langle\hat{H}_{\rm SO}\rangle|^2_{\mathbf{M}//\mathbf{e}_x} - |\langle\hat{H}_{\rm SO}\rangle|^2_{\mathbf{M}//\mathbf{e}_z}\}$.

	$\lvert z^2\uparrow\rangle$	$\lvert z^2\downarrow\rangle$	$\lvert xz\uparrow\rangle$	$\lvert yz\uparrow\rangle$	$\lvert xz\downarrow\rangle$	$\lvert yz\downarrow\rangle$	$\lvert xy\uparrow\rangle$	$\lvert x^2-y^2\uparrow\rangle$	$\lvert xy\downarrow\rangle$	$\lvert x^2-y^2\downarrow\rangle$
$\langle z^2\uparrow\rvert$				$3\frac{\xi\hbar^2}{2}$		$-3\frac{\xi\hbar^2}{2}$				
$\langle z^2\downarrow\rvert$				$-3\frac{\xi\hbar^2}{2}$		$3\frac{\xi\hbar^2}{2}$				
$\langle xz\uparrow\rvert$				$-\frac{\xi\hbar^2}{2}$		$\frac{\xi\hbar^2}{2}$	$\frac{\xi\hbar^2}{2}$		$-\frac{\xi\hbar^2}{2}$	
$\langle yz\uparrow\rvert$	$3\frac{\xi\hbar^2}{2}$	$-3\frac{\xi\hbar^2}{2}$	$-\frac{\xi\hbar^2}{2}$		$\frac{\xi\hbar^2}{2}$			$\frac{\xi\hbar^2}{2}$		$-\frac{\xi\hbar^2}{2}$
$\langle xz\downarrow\rvert$				$\frac{\xi\hbar^2}{2}$		$-\frac{\xi\hbar^2}{2}$	$-\frac{\xi\hbar^2}{2}$		$\frac{\xi\hbar^2}{2}$	
$\langle yz\downarrow\rvert$	$-3\frac{\xi\hbar^2}{2}$	$3\frac{\xi\hbar^2}{2}$	$\frac{\xi\hbar^2}{2}$		$-\frac{\xi\hbar^2}{2}$			$-\frac{\xi\hbar^2}{2}$		$\frac{\xi\hbar^2}{2}$
$\langle xy\uparrow\rvert$			$\frac{\xi\hbar^2}{2}$		$-\frac{\xi\hbar^2}{2}$			$-4\frac{\xi\hbar^2}{2}$		$4\frac{\xi\hbar^2}{2}$
$\langle x^2-y^2\uparrow\rvert$				$\frac{\xi\hbar^2}{2}$		$-\frac{\xi\hbar^2}{2}$	$-4\frac{\xi\hbar^2}{2}$		$4\frac{\xi\hbar^2}{2}$	
$\langle xy\downarrow\rvert$			$-\frac{\xi\hbar^2}{2}$		$\frac{\xi\hbar^2}{2}$			$4\frac{\xi\hbar^2}{2}$		$-4\frac{\xi\hbar^2}{2}$
$\langle x^2-y^2\downarrow\rvert$				$-\frac{\xi\hbar^2}{2}$		$\frac{\xi\hbar^2}{2}$	$4\frac{\xi\hbar^2}{2}$		$-4\frac{\xi\hbar^2}{2}$	

APPENDIX: CORRECTION TO THE GROUND-STATE ENERGY DUE TO SPIN-ORBIT COUPLING, AS A FUNCTION OF Δm_l AND Δm_s

In this Appendix, we describe how the contribution of a given virtual transition to the correction of the ground-state energy can be calculated using the second-order perturbation theory. This will indicate if the virtual transition promotes in-plane or out-of-plane anisotropy. We consider only the d orbitals of a single atom and ignore hybridization. We also consider that the crystal field (which describes the interface or the surface perpendicular to the Oz quantization axis) and the exchange interaction have clearly split the d_{z^2}, d_{xz}, d_{yz}, d_{xy}, and $d_{x^2-y^2}$ orbitals with spin $\uparrow$ and $\downarrow$. We wish to calculate the matrix elements of the spin-orbit-coupling Hamiltonian between one occupied and one unoccupied of these states.

For the orbital quantum number $l = 2$ (d orbitals), we must first express the $|m_l,m_s\rangle$ states where $m_l = 0,\pm1,\pm2$ and $m_s = \pm\frac{1}{2}$ on the basis of the states $|J,M_J\rangle$ eigenvectors of the atom central part and spin-orbit-coupling Hamiltonian, using the Clebsh-Gordan coefficients. The spin-orbit-coupling Hamiltonian is given by $\hat{H}_{\rm SO} = \xi\hat{\mathbf{L}}\cdot\hat{\mathbf{S}}$, where ξ is a spin-orbit-coupling parameter. $\hat{\mathbf{L}}$ and $\hat{\mathbf{S}}$ are the angular momentum and spin operators. Using the total angular momentum $\hat{\mathbf{J}} = \hat{\mathbf{L}} + \hat{\mathbf{S}}$ and the matrix elements of $\hat{H}_{\rm SO}$ between $|J,M_J\rangle$ states, we can express the matrix elements of $\hat{H}_{\rm SO}$ between $|m_l,m_s\rangle$ states. The next step consists in writing the d orbitals $|d_i,m_s\rangle$ in the basis of the $|m_l,m_s\rangle$ states as $|z^2,\pm\frac{1}{2}\rangle = |0,\pm\frac{1}{2}\rangle$, $|yz,\pm\frac{1}{2}\rangle = \frac{i}{\sqrt{2}}\{|-1,\pm\frac{1}{2}\rangle + |1,\pm\frac{1}{2}\rangle\}$, $|xz,\pm\frac{1}{2}\rangle = \frac{1}{\sqrt{2}}\{|-1,\pm\frac{1}{2}\rangle - |1,\pm\frac{1}{2}\rangle\}$, $|xy,\pm\frac{1}{2}\rangle = \frac{i}{\sqrt{2}}\{|-2,\pm\frac{1}{2}\rangle - |2,\pm\frac{1}{2}\rangle\}$, and $|x^2-y^2,\pm\frac{1}{2}\rangle = \frac{1}{\sqrt{2}}\{|-2,\pm\frac{1}{2}\rangle + |2,\pm\frac{1}{2}\rangle\}$. This allows us to calculate the matrix elements of the spin-orbit-coupling Hamiltonian between $|d_i,m_s\rangle$ states (see Table II).

In the last step, we express the electron states spin-polarized in the direction parallel or perpendicular to the Oz axis. To do this, we use the fact that the average value of the $\hat{S}_x$, $\hat{S}_y$, and $\hat{S}_z$ operators is $\pm\frac{\hbar}{2}\sin\theta$, 0, and $\frac{\hbar}{2}\cos\theta$, respectively, for the spin state $[\cos\frac{\theta}{2}|+\frac{1}{2}\rangle \pm \sin\frac{\theta}{2}|-\frac{1}{2}\rangle]$. Consequently, the states $|+\frac{1}{2}\rangle$ and $|-\frac{1}{2}\rangle$ descibe the $\uparrow$ and $\downarrow$ spin states polarized along the Oz axis (this axis being perpendicular to the surface or interface), while the states $\frac{1}{\sqrt{2}}\{|+\frac{1}{2}\rangle + |-\frac{1}{2}\rangle\}$ and $\frac{1}{\sqrt{2}}\{|+\frac{1}{2}\rangle - |-\frac{1}{2}\rangle\}$ correspond, respectively, to the $\uparrow$ and $\downarrow$ spin states polarized along Ox (this axis being parallel to the interface or to the surface).

The $|d_i\uparrow\downarrow\rangle$ states can further be expressed in terms of $|d_i,m_s\rangle$ states: we get $|d_i\uparrow\rangle = |d_i,+\frac{1}{2}\rangle$ and $|d_i\downarrow\rangle = |d_i,-\frac{1}{2}\rangle$ when the spin polarization is along Oz and $|d_i\uparrow\rangle = \frac{1}{\sqrt{2}}\{|d_i,+\frac{1}{2}\rangle + |d_i,-\frac{1}{2}\rangle\}$ and $|d_i\downarrow\rangle = \frac{1}{\sqrt{2}}\{|d_i,+\frac{1}{2}\rangle - |d_i,-\frac{1}{2}\rangle\}$ when the spin polarization is along Ox. This can be used to calculate the matrix elements to the spin-orbit-coupling Hamiltonian between $|d_i\uparrow\downarrow\rangle$ states. These matrix elements will depend on the direction of the spin polarization, along Oz or along Ox. Table III gives the difference between the square moduli of these matrix elements calculated for each of these two directions. Negative terms in this table correspond to virtual transitions which promote magnetization along Oz (perpendicular to the interface or surface).

*Corresponding author: calmels@cemes.fr

[1]M. T. Johnson, P. J. H. Bloemen, F. J. A. den Broeder, and J. J. de Vries, Rep. Prog. Phys. **59**, 1409 (1996).
[2]L. Berger, Phys. Rev. B **54**, 9353 (1996).
[3]J. C. Slonczewski, J. Magn. Magn. Mater. **159**, L1 (1996).
[4]M. Tsoi, A. G. M. Jansen, J. Bass, W.-C. Chiang, M. Seck, V. Tsoi, and P. Wyder, Phys. Rev. Lett. **80**, 4281 (1998).
[5]E. B. Myers, D. C. Ralph, J. A. Katine, R. N. Louie, and R. A. Buhrman, Science **285**, 867 (1999).
[6]J. Z. Sun, J. Magn. Magn. Mater. **202**, 157 (1999).
[7]J. A. Katine, F. J. Albert, R. A. Buhrman, E. B. Myers, and D. C. Ralph, Phys. Rev. Lett. **84**, 3149 (2000).
[8]Y. Jiang, T. Nozaki, S. Abe, T. Ochiai, A. Hirohata, N. Tezuka, and K. Inomata, Nat. Mater. **3**, 361 (2004).

[9] S. Urazhdin, N. O. Birge, W. P. Pratt, and J. Bass, Appl. Phys. Lett. **84**, 1516 (2004).
[10] P. M. Braganca, I. N. Krivorotov, O. Ozatay, A. G. F. Garcia, N. C. Emley, J. C. Sankey, D. C. Ralph, and R. A. Buhrman, Appl. Phys. Lett. **87**, 112507 (2005).
[11] A. Kent, B. Ozyilmaz, and E. del Barco, Appl. Phys. Lett. **84**, 3897 (2004).
[12] K. J. Lee, O. Redon, and B. Dieny, Appl. Phys. Lett. **86**, 022505 (2005).
[13] S. Mangin, D. Ravelosona, J. A. Katine, M. J. Carey, B. D. Terris, and E. E. Fullerton, Nat. Mater. **5**, 210 (2006).
[14] T. Seki, S. Mitani, K. Yakushiji, and K. Takanashi, Appl. Phys. Lett. **88**, 172504 (2006).
[15] H. Meng and J.-P. Wang, Appl. Phys. Lett. **88**, 172506 (2006).
[16] P. F. Carcia, A. D. Meinhaldt, and A. Suna, Appl. Phys. Lett. **47**, 178 (1985).
[17] H. J. G. Draaisma, W. J. M. de Jonge, and F. J. A. den Broeder, J. Magn. Magn. Mater. **66**, 351 (1987).
[18] S. Hashimoto, Y. Ochiai, and K. Aso, J. Appl. Phys. **66**, 4909 (1989).
[19] F. J. A. den Broeder, D. Kuiper, H. C. Donkersloot, and W. Hoving, Appl. Phys. A **49**, 507 (1989).
[20] F. J. A. den Broeder, W. Hoving, and P. J. H. Bloemen, J. Magn. Magn. Mater. **93**, 562 (1991).
[21] B. N. Engel, C. D. England, R. A. Van Leeuwen, M. H. Wiedmann, and C. M. Falco, Phys. Rev. Lett. **67**, 1910 (1991).
[22] W. B. Zeper, F. J. A. M. Greidanus, P. F. Carcia, and C. R. Fincher, J. Appl. Phys. **65**, 4971 (1989).
[23] C.-J. Lin, G. L. Gorman, C. H. Lee, R. F. C. Farrow, E. E. Marinero, H. V. Do, H. Notarys, and C. J. Chien, J. Magn. Magn. Mater. **93**, 194 (1991).
[24] G. H. O. Daalderop, P. J. Kelly, and F. J. A. den Broeder, Phys. Rev. Lett. **68**, 682 (1992).
[25] K. Kyuno, J.-G. Ha, R. Yamamoto, and S. Asano, Jpn. J. Appl. Phys. **35**, 2774 (1996).
[26] M. T. Johnson, J. J. de Vries, N. W. E. McGee, J. aan de Stegge, and F. J. A. den Broeder, Phys. Rev. Lett. **69**, 3575 (1992).
[27] M. T. Johnson, F. J. A. den Broeder, J. J. de Vries, N. W. E. McGee, R. Jungblut, and J. aan de Stegge, J. Magn. Magn. Mater. **121**, 494 (1993).
[28] Y. B. Zhang, J. A. Woollam, Z. S. Shan, J. X. Shen, and D. J. Sellmyer, IEEE Trans. Magn. **30**, 4440 (1994).
[29] J.-M. L. Beaujour, W. Chen, K. Krycka, C.-C. Kao, J. Z. Sun, and A. D. Kent, Eur. Phys. J. B **59**, 475 (2007).
[30] S. Girod, M. Gottwald, S. Andrieu, S. Mangin, J. McCord, E. E. Fullerton, J.-M. L. Beaujour, B. J. Krishnatreya, and A. D. Kent, Appl. Phys. Lett. **94**, 262504 (2009).
[31] M. Gottwald, S. Girod, S. Andrieu, and S. Mangin, IOP Conf. Ser.: Mater. Sci. Eng. **12**, 012018 (2010).
[32] S. Mangin, Y. Henry, D. Ravelosona, J. A. Katine, and E. E. Fullerton, Appl. Phys. Lett. **94**, 012502 (2009).
[33] W. Chen, J.-M. L. Beaujour, G. de Loubens, and A. D. Kent, Appl. Phys. Lett. **92**, 012507 (2008).
[34] S. Mizukami, X. Zhang, T. Kubota, H. Naganuma, M. Oogane, Y. Ando, and T. Miyazaki, Appl. Phy. Express **4**, 013005 (2011).
[35] J. M. Shaw, H. T. Nembach, and T. J. Silva, Appl. Phys. Lett. **99**, 012503 (2011).
[36] F. Gimbert, L. Calmels, and S. Andrieu, Phys. Rev. B **84**, 094432 (2011).
[37] Z. Li, Z. Zhang, H. Zhao, B. Ma, and Q. Y. Jin, J. Appl. Phys. **106**, 013907 (2009).
[38] L. You, R. C. Sousa, S. Bandiera, B. Rodmacq, and B. Dieny, Appl. Phys. Lett. **100**, 172411 (2012).
[39] M. Gottwald, S. Andrieu, F. Gimbert, E. Shipton, L. Calmels, C. Magen, E. Snoeck, M. Liberati, T. Hauet, E. Arenholz, S. Mangin, and E. E. Fullerton, Phys. Rev. B **86**, 014425 (2012).
[40] P. Blaha, K. Schwarz, G. K. H. Madsen, D. Kvasnicka, and J. Luits, *Wien2k, An Augmented Plane Wave + Local Orbitals Program for Calculating Crystal Properties* (K. Schwarz, Vienna, Austria, 2001).
[41] J. P. Perdew and Y. Wang, Phys. Rev. B **45**, 13244 (1992).
[42] I. Galanakis, M. Alouani, and H. Dreysse, Phys. Rev. B **62**, 6475 (2000).
[43] J. M. Gallego, S. Kim, T. J. Moran, D. Lederman, and I. K. Schuller, Phys. Rev. B **51**, 2550 (1995).
[44] H. Zabel and S. D. Bader, *Magnetic Heterostructures: Advances and Perspectives in Spin Structures and Spin Transport* (Springer, Berlin, 2007).
[45] J. Stöhr, J. Magn. Magn. Mater. **200**, 470 (1999).
[46] P. Bruno, Phys. Rev. B **39**, 865 (1989).
[47] A. R. Mackintosh and O. K. Andersen, *Electrons at the Fermi Surface* (Cambridge University Press, Cambridge, 1980).
[48] J. Stöhr, J. Electron Spectrosc. Relat. Phenom. **75**, 253 (1995).
[49] A. Lessard, T. H. Moos, and W. Hübner, Phys. Rev. B **56**, 2594 (1997).
[50] G. H. O. Daalderop, P. J. Kelly, and M. F. H. Schuurmans, Phys. Rev. B **50**, 9989 (1994).
[51] A. Lehnert, S. Dennler, P. Blonski, S. Rusponi, M. Etzkorn, G. Moulas, P. Bencok, P. Gambardella, H. Brune, and J. Hafner, Phys. Rev. B **82**, 094409 (2010).